Pore-to-Pore Hopping Model for the Interpretation of the Pulsed Gradient Spin Echo Attenuation of Water Diffusion in Cell Suspension Systems

Pang-Chih Jiang,* Tsyr-Yan Yu,* Wann-Cherng Perng,† and Lian-Pin Hwang*
*Department of Chemistry, National Taiwan University and Institute of Atomic and Molecular Sciences, Academia Sinica, and
†Department of Medicine, Tri-Service General Hospital, National Defense Medical Center, Taipei, Taiwan, Republic of China

ABSTRACT A simplified pore-to-pore hopping model for the two-phase diffusion problem is developed for the analysis of the pulsed gradient spin echo (PGSE) attenuation of water diffusion in the condensed cell suspension systems. In this model, the two phases inside and outside the cells are treated as two different kinds of pores, and the spin-bearing molecules perform hopping diffusion between them. The size and the orientations of those two respective pores are considered, and then the diffraction pattern of the PGSE attenuation may be well simulated. Nevertheless, the intensity of the characteristic peak decreases with increasing membrane permeability, from which the exchange time may be estimated. We then analyze the experimental ^{1}H PGSE results of the erythrocytes suspension system. The water-residence lifetime in the erythrocyte is obtained to be 10 ms, which is the same as that estimated from the two-region approximation. Furthermore, the PGSE attenuation curve of addition of p-Chloromercuribenzenesulfonate (p-CMBS) is also discussed. It predicts that the alignment of erythrocytes will become normal to the magnetic field direction after the addition of p-CMBS, and inspection using a light microscope confirms that result.

INTRODUCTION

Pulsed field gradient spin echo (PGSE) nuclear magnetic resonance technique has been used to probe the structures of porous materials and the diffusion of the confined spin-bearing molecules (Tanner and Stejskal, 1968; Callaghan, 1991). It is well known that, in **q** space experiments there are diffraction-like patterns shown in the PGSE attenuation curves for various cases of restricted diffusion (Callaghan et al., 1991; Balinov et al., 1994; Kuchel et al., 1997; Callaghan, 1995; Codd and Callaghan, 1999). For restricted diffusion in single pores, the characteristic diffraction-like pattern may reflect the size of the pore, whereas, for restricted diffusion among well-separated multipores, the patterns reflect the mean distance between the pores.

Kärger (1985) developed an analytical approach to examining PGSE attenuation through two-region exchange approximation. Because there is exchange between two freely diffusing phases, the calculated double exponential decay profile does not display the diffraction-like pattern as observed in the PGSE experiment on the erythrocyte suspension system. Stanisz et al. (1998) modified Kärger's interpretation for the PGSE attenuation of the erythrocyte suspension, in which they considered the diffusion within an erythrocyte as one-dimensional restricted diffusion. They also estimated an apparent diffusion coefficient from the PGSE attenuation feature by considering one-dimensional restricted diffusion and then calculated the profile of PGSE attenuation using the two-region exchange model. Similarly, Price et al. (1998) derived the apparent diffusion coefficient from the PGSE attenuation of the restricted diffusion in a spherical pore. Also, Peled et al. (1999) applied the same strategy to studying water diffusion in the frog sciatic nerve and derived the apparent diffusion coefficient from the PGSE attenuation in a cylindrical pore to mimic the restricted diffusion in the nerve cells. All those results involve the usage of the apparent diffusion coefficient to illustrate the effects of the restricted diffusion in the cells and, in turn, to explain the diffraction-like pattern of the PGSE attenuation curve.

Kuchel et al. (1997) explored the PGSE experiments for the erythrocytes suspension system and estimated two physically significant lengths from the two diffraction-like patterns of the attenuation profile. They assigned the two lengths obtained to the size of the erythrocyte and the average distance of extracellular pore spacing. Such a treatment is similar to that adopted by Callaghan et al. (1991) for the pore-like space between the polystyrene spheres. They have used this method to derive the PGSE attenuation for the restricted diffusion among multipores of the same size. Also, they introduced an effective diffusion coefficient to describe self-diffusion for long-range migration between pores. The formulation used by Stanisz et al., (1998), Peled et al., (1999), and Price et al., (1998) can be used to interpret the diffraction-like pattern caused by the restricted diffusion in the erythrocytes, but it cannot be used to explain the first diffusion-like peak observed by Kuchel et al. (1997). It implies that there exists some constraint in extracellular diffusion. Therefore, a new model is needed to include the effects of the size and the arrangement of the erythrocytes and the external pores between the erythrocytes. Because such systems are too complicated to be solved exactly by the general diffusion equation, the modified pore-to-pore

Received for publication 5 July 2000 and in final form 18 March 2001.
Address reprint request to Lian-Pin Hwang, National Taiwan University, Department of Chemistry, 1 Roosevelt Rd., Sect. 4, P.O. Box 23-34, Taipei, Taiwan, Republic of China. Tel.: 886-2-2366-8287; Fax: +886-2-2362-0200; Email: nmra@po.iams.sinica.edu.tw.

0006-3495/01/06/2493/12 $2.00

hopping model may be used as an approximation for studying the diffusions in the erythrocyte suspension system.

In the present work, we develope a simplified diffusion model for a two-phase system, represented by the coupled master equations (Haus and Kehr, 1987) with pore-to-pore hopping exchange between two different pores. We take into account the effects of the pore size, the spatial arrangement of the pores, and the variation of water-residing times in each phase on the PGSE attenuation. Then we calculate the PGSE attenuation of diffusion among multipores of the same size and compare the results with those derived by Callaghan (1995). Also, we applied the proposed model to analyzing the results of the PGSE experiments for the erythrocyte suspension system.

THEORY

The general formulation

The formulation of the PGSE attenuation for the molecular diffusion among multipores can be easily derived based on the "pore equilibrium" condition (Callaghan et al. 1991). This assumption is suitable for a porous medium with well-defined pore–channel structure, i.e., the size of the channels is much smaller than that of the pores. With the pore equilibrium condition and the short gradient pulse approximation (Tanner and Stejskal, 1968; Linse and Söderman, 1995), where the waveform of the gradient pulse is considered to be a δ-function in time domain, the PGSE attenuation of diffusion among multi-identical pores can be expressed in **q** space by (Callaghan, 1991)

$$\begin{aligned} E(\mathbf{q}, \Delta) &= \sum_n \int_{V_0} dr_0 \int_{V_n} dr_n \rho(r_0) \frac{P(n,\Delta)}{V} \\ &\quad \times \exp[i2\pi q \cdot (r_n + R_n - r_0)] \\ &= S^*(q) S(q) P(\mathbf{q}, \Delta), \end{aligned} \tag{1}$$

where $\mathbf{q} = \gamma\delta\mathbf{G}/2\pi$, γ is the gyromagnetic ratio, δ is the duration of the magnetic field gradient pulses, $\mathbf{G}$ is the strength of the gradient; and $\rho(\mathbf{r}_0)$ is the density of the spins within the 0th pore initially, and Δ is the interval between the two pulsed gradients. The subscript 0 represents the 0th pore, e.g., the pore where the spin is situated at the initial time, and the subscript n indicates the nth pore where the spin is situated at time Δ. V_0 and V_n are the internal space of the 0th and the nth pores, respectively. $\mathbf{r}_0$ and $\mathbf{r}_n$ are the position vectors of the pore centers at the 0th and the nth pores, respectively. In Eq. 1, $S(q) \equiv \int_V d\mathbf{r}(1/V)\exp(i2\pi\mathbf{q} \cdot \mathbf{r})$ is called the "structure factor" of the pore, where $1/V$ is the density of the spins, which normalizes the amount of the spins in a pore, and V is the volume of a single pore. $P(n, \Delta)$ is the probability of a spin existing in the nth pore at time Δ, $\mathbf{R}_n$ is the position vector of the center of the nth pore relative to that of the 0th pore, and

$$P(\mathbf{q}, \Delta) = \sum_n P(n, \Delta)\exp(i2\pi\mathbf{q} \cdot \mathbf{R}_n). \tag{2}$$

Thus $P(\mathbf{q}, \Delta)$ describes the arrangement of the pores as expressed in **q** space, and one may derive it in terms of the hopping exchange model described in the master equation in the next section.

Diffusion among identical pores

For restricted diffusion in a single pore with a permeable wall, one may treat the boundary as a semi-adsorptive wall (Barzykin et al. 1995),

$$D \frac{\partial P(\mathbf{r}_0|\mathbf{r}, t)}{\partial r} + H \cdot P(\mathbf{r}_0|\mathbf{r}, t|_{r=a} = 0, \tag{3}$$

where D is the diffusion coefficient, H is a constant to represent the transport ability of the boundary; $\mathbf{r}_0$ and $\mathbf{r}$ are the position vectors; $P(\mathbf{r}_0|\mathbf{r}, t)$ is the probability of finding a particle initially at r_0 and at r after a time t, and a represents the position where the boundary exists. By solving the diffusion equation with the boundary condition described by Eq. 3, the total probability within the pore, e.g., $\int_V dr P(r_0|r, t)$, gives an exponential decay form with a characteristic lifetime. By analogy, we adopted the same idea to the case of the exchange diffusion among multipores and take the lifetime as the time needed to travel from one pore to another. Then, the master equation, which is analogous to that of the multisite jump diffusion (Haus and Kehr 1987), can be constructed. The master equation of hopping diffusion among pores of the same size can be written as

$$\frac{\partial P_i(t)}{\partial t} = \sum_{j=1}^{N} W P_{ij}(t) - NW P_i(t), \tag{4}$$

where $P_i(t)$ is the probability of a spin existing at the ith pore at time t, $P_{ij}(t)$ is the joint probability of a spin existing at the jth pore neighboring to the ith pore, N is the number of the first shell of pores, and $W = 1/N\tau$ is the pore-to-pore exchange rate, where τ is the spin residence lifetime in a pore.

In Eq. 2, $P(\mathbf{q}, t = \Delta)$ may be obtained readily by the Fourier–Laplace transform of Eq. 4 and then solved by inverse Laplace transform, which yields

$$\begin{aligned} P(\mathbf{q}, \Delta) &= \exp[-\Delta \cdot NW(1 - A[\mathbf{q}])] \\ &= \exp\left[-\frac{\Delta}{\tau_j}(1 - A[\mathbf{q}])\right], \end{aligned} \tag{5}$$

where

$$A[\mathbf{q}] \equiv \frac{1}{N}\sum_{j=1}^{N}\exp(i2\pi\mathbf{q}\cdot\mathbf{R}_j)$$

is called the configuration integral of this multipore system and $\mathbf{R}_j$ is the position vector of the center of the *j*th pore in the first shell relative to that of the central pore.

Equation 5 was in the same form as that derived previously by Callaghan et al. (1991), except that the term Δ/τ_j is replaced by $D_{eff}\Delta/6l^2$ in their formulation, where D_{eff} is the long-time limit (effective) diffusion coefficient among the pores, and l is the distance between two pores.

Application to cell suspension systems

The formulation may be extended with the help of Eq. 1 to condensed cell suspension systems. As shown in Fig. 1, the condensed cell suspension system can be approximated as a system consisting of two kinds of pores. We denote the cells as pores C. The space enclosed by the cells can be considered as the external pores, which are denoted as pores S. One may suppose that the diffusion of spin-bearing molecules starting from a pore C (or S) initially can be found either in a pore C or in a pore S at time Δ, and thus four cases must be considered. Particularly, for those spins existing in pores C initially, and at a later time Δ in pores S, the contribution to the magnetization is given by

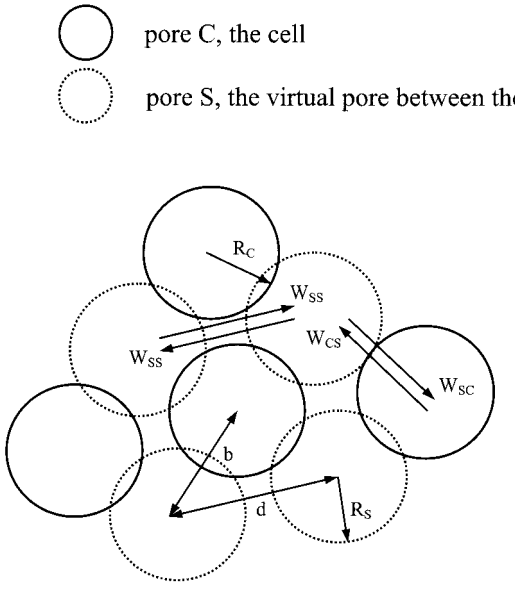

FIGURE 1 The pictorial representation of the simplified two-phase model consisting of the cells (*solid circle*, pores C, solid line represents the membrane) and the pores between the cells (*dotted circle*, pores S). R_C and R_S are the radius of pores C and pores S, respectively. The mean distance between two pores S is *d*. The mean distance between a pore C and a pore S is *b*. The hopping rates between pores are also marked by *W* with appropriate subscripts to indicated the exchanging species.

$$M_{C\to S}(\mathbf{q},\Delta) = S_C(\mathbf{q},\Delta) \times \int_{V_C} d\mathbf{r}_C\rho(\mathbf{r}_C)\int_{V_S} d\mathbf{r}_S\frac{1}{V_S}\exp[i2\pi\mathbf{q}\cdot(\mathbf{r}_S-\mathbf{r}_C)], \quad (6)$$

where

$$S_C(\mathbf{q},\Delta) = \sum_n S_C(n,\Delta)\exp(i2\pi\mathbf{q}\cdot\mathbf{R}_{Sn}), \quad (7)$$

and where $S_C(n,\Delta)$ is the probability for a spin diffusing from a pore C initially to the *n*th pore S at time Δ. $\mathbf{R}_{Sn}$ is the position vector at the center of the *n*th pore S relative to that of the initial pore C. V_C and V_S are the volumes of a single pore C and pore S, respectively. $\mathbf{r}_C$ and $\mathbf{r}_S$ are the position vectors within a pore C and a pore S relative to their pore centers, respectively. The expressions for the other cases, C→C (pore C to pore C), S→C and S→S are similar. Here, the subscript C means the starting point is a pore C, and the subscript S means the starting point is a pore S. There are only three hopping rate constants considered in this system because the cells do not connect to each other directly. Pores S are all connected to their neighboring pores S with a hopping rate of W_{SS}. Pores C are isolated from the other pores C, but are connected to their neighboring pores S with hopping rate constants $W_{CS} = 1/(N\tau_C)$ and $W_{SC} = 1/(N\tau_S)$, where τ_C and τ_S are the spin residence lifetimes of pores C and pores S, respectively.

Furthermore, in the PGSE experiment, the time interval between the two gradient pulses is set shorter than the transverse spin relaxation, and the observed magnitudes of PGSE attenuation for various q is normalized by the observed value at $q = 0$. Thus, for this simplified system, the effect of the transverse spin relaxation processes is cancelled. The master equation may be written without the spin relaxation term as

$$\frac{\partial C_n(t)}{\partial t} = \sum_{i=1}^{N} W_{SC}S_{ni}(t) - NW_{CS}C_n(t), \quad (8a)$$

$$\frac{\partial S_n(t)}{\partial t} = \sum_{i=1}^{M} W_{SS}S_{ni}(t) + \sum_{i=1}^{N} W_{CS}C_{ni}(t) - (NW_{SC} + MW_{SS})S_n(t), \quad (8b)$$

where $C_n(t)$, $S_n(t)$, $C_{ni}(t)$, and $S_{ni}(t)$ are the corresponding probabilities at time t, N is the coordination number of a pore C surrounded by S pores, and M is that of a pore S surrounded by other S pores. For simplicity, we set the same value N as the coordination number of a pore S surrounded by pores C. Then we follow the hopping exchange model and obtain $C_C(\mathbf{q},\Delta)$, $S_C(\mathbf{q},\Delta)$, $C_S(\mathbf{q},\Delta)$, and $S_S(\mathbf{q},\Delta)$ by solving the coupled master equation after the Fourier–Laplace transform and the inverse Laplace transform as

derived in the Appendix. $M_{C\to S}$ may be calculated in accordance with Eq. 6. By analogy, $M_{C\to C}$, $M_{S\to C}$, and $M_{S\to S}$ can be obtained accordingly. Consequently, for random pore arrangement, we obtain

$$C_C(\mathbf{q}, \Delta) = x_{CC}\exp(\lambda_1\Delta) + y_{CC}\exp(\lambda_2\Delta), \quad (9a)$$

$$S_C(\mathbf{q}, \Delta) = x_{SC}\exp(\lambda_1\Delta) + y_{SC}\exp(\lambda_2\Delta), \quad (9b)$$

$$C_S(\mathbf{q}, \Delta) = x_{CS}\exp(\lambda_1\Delta) + y_{CS}\exp(\lambda_2\Delta), \quad (9c)$$

$$S_S(\mathbf{q}, \Delta) = x_{SS}\exp(\lambda_1\Delta) + y_{SS}\exp(\lambda_2\Delta), \quad (9d)$$

where the parameters x_i and y_i (i = CC, SC, CS, and SS) are defined in the Appendix. They are related to the hopping rate and the pore-to-pore distance. The exponent parameters, λ_1, and λ_2, in Eqs. 9 are given by

$$\lambda_{1,2} \equiv \frac{-(NW_{CS} + \alpha) \pm \sqrt{(NW_{CS} - \alpha)^2 + 4N^2W_{CS}W_{SC}\mathrm{sinc}^2(2\pi qb)}}{2} \quad (10)$$

where α is defined by

$$\alpha = NW_{SC} + MW_{SS}[1 - \mathrm{sinc}(2\pi qd)]. \quad (11)$$

On the basis of the completely random arrangement of pore C and pore S, the derivation procedures are readily presented in the Appendix. By summing up the four parts as given in Eq. 9, we obtain the PGSE attenuation

$$E(q, \Delta) = \frac{1}{V_C + V_S}\left\{\left[\frac{x_{CC}}{V_C}F_C^2 + \left(\frac{x_{SC}}{V_S} + \frac{x_{CS}}{V_C}\right)F_CF_S + \frac{x_{SS}}{V_S}F_S^2\right] \times \exp(\lambda_1\Delta) + \left[\frac{y_{CC}}{V_C}F_C^2 + \left(\frac{y_{SC}}{V_S} + \frac{y_{CS}}{V_C}\right)F_CF_S + \frac{y_{SS}}{V_S}F_S^2\right]\exp(\lambda_2\Delta)\right\}, \quad (12)$$

where the structure integral for a single pore C and a single pore S are given by

$$F_C \equiv \int_{V_C} d\mathbf{r}_C \exp(i2\pi\mathbf{q}\cdot\mathbf{r}_C)$$

and

$$F_S \equiv \int_{V_S} d\mathbf{r}_S \exp(i2\pi\mathbf{q}\cdot\mathbf{r}_S),$$

respectively. $1/(V_C + V_S)$ is the density of the spins, which normalizes the amount of the spins in one pair of pore C and pore S.

MATERIALS AND METHODS

Preparation of erythrocyte suspension

Blood was obtained from a healthy human volunteer. The erythrocytes were centrifugally washed (3000 × g, 10 min) two times in cold glucose-enriched saline solution (154 mM NaCl, 10 mM glucose, 4°C). The plasma and the buffy coat were discarded. The appropriate amount of cold glucose-enriched saline solution was then added to form the erythrocyte suspension. All erythrocyte suspensions were gently bubbled with carbon monoxide for 5 min to transform the hemoglobin into a stable low-spin diamagnetic state. For the experiments on inhibiting transmembrane water exchange, p-Chloromercuribenzenesulfonate (p-CMBS) (Sigma, St. Louis, MO) was added (1.9 mg to 1 ml of suspension) and the suspension was kept at 37°C for 1 hr before doing the PGSE experiments.

PGSE experiment

PGSE experiments were performed on a (Bruker Analytik GmbH, Rheinsteuen, Germany) MSL-500 spectrometer, operating at a 11.4-T magnetic field, equipped with a Bruker DIFF-25 gradient probe capable of a maximum gradient of 10 T m^{-1}. The use of the actively shielded gradient coil in the probe and the precompensation function of preemphasis unit greatly reduce the effect of eddy current on diffusion measurements. A blanking unit is open 200 μs before the gradient pulse and stays on during the gradient pulse and the ring-down period to allow the preemphasis to work. The eddy current generated after the gradient pulse is less than 2% of the static value of the gradient pulse within 150 μs. It rings down to less than 1% after 250 μs. In all the experiments, the standard PGSE pulse sequence and phase cycles were used (Kuchel et al., 1997). The duration of the 90° pulse was 25 μs; that of the two gradient pulses, δ, was 1.2 or 2 ms. Because the proton transverse relaxation times inside and outside the erythrocyte (Stanisz et al., 1998) yield 160 and 400 ms, respectively, to achieve significant signal in our experiments, one may set the time interval between the two gradient pulses to be shorter than 160 ms. Here the time interval between the gradient pulses was set to 15 or 40 ms. The relaxation delay between transients was 8 s; and the number of transients per spectrum was 80. The probe temperature was maintained at 298 ± 0.3 K to minimize the convection. The S/N for full magnetization was higher than 2000 in all the experiments.

Orientation observation

Gelatin solution was prepared by adding an appropriate amount of gelatin (Sigma, St. Louis, MO) into a saline solution. The erythrocyte suspensions (with or without p-CMBS treatment) were added to the gelatin solution and kept at 37°C for at least 3 h within the 11.4-T magnetic field to ensure the

formation of gelatin network so that the erythrocytes could become readily oriented. For the controlled experiments, the samples were kept outside the magnetic field. The temperature was then cooled to 20°C to make the sample gel. The orientation of the erythrocytes fixed in the gelatin gel was observed under a light microscope (original magnification ×400).

RESULTS AND DISCUSSION

Permeability effect

Considering the condensed spherical cell (pores C) suspension systems, the pores (pores S) between pores C may also be approximated to be a sphere, as shown in Fig. 1. For the case with the volume ratio of pore C to pore S to be V_C:V_S = 0.7, we obtain the radius ratio of pore C to pore S, R_C:$R_S = \sqrt[3]{0.7}$. The mean distance b between pore C and pore S may be approximated by the sum of their radii because of the compact stacking of the two kinds of pores (see Fig. 1). Moreover, if one considers the 3-dimensional cubic packing of two kinds of pores, the mean distance d between two S pores may be set to $\sim\sqrt{3}b$. Here the same density of spins is assigned to each pore, i.e., $\rho_C/\rho_S = 1.0$, and thus the population ratio of the spins in pore C to pore S gives $P_C/P_S = V_C\rho_C/V_S\rho_S = 0.7$, which also implies the ratio of the two rate constants $W_{SC}/W_{CS} = P_C/P_S = 0.7$ in accordance with the principle of detailed balance. Then, we set $\Delta = 1.5/MW_{SS}$, which is 1.5 times the lifetime of a spin in pore S. In the present work, we first considered a situation in which the spin-bearing molecules may not penetrate the cell membrane, e.g., $W_{CS} = W_{SC} = 0$, but $W_{SS} \neq 0$ because there must be connections between pores S. In this case, we obtain $\exp(\lambda_1\Delta) = 1$ and $\lambda_2 = -MW_{SS}[1 - \mathrm{sinc}(qd)]$. Consequently, the attenuation reduces to

$$E(k, \Delta) = \frac{1}{V_C + V_S}\left[\frac{F_C^2}{V_C} + \frac{F_S^2}{V_S}\exp(\lambda_2\Delta)\right], \qquad (13)$$

where the first part, $F_C^2/[V_C(V_C + V_S)]$, results solely from the restricted molecular diffusion in pores C, and the second part, $F_S^2\exp(\lambda_2\Delta)/[V_S(V_C + V_S)]$, from the molecular diffusion in the external pores. Furthermore, one may enhance W_{SC} and W_{CS} to the same magnitude of W_{SS} to investigate the effect of the permeability. However, when W_{SC} and W_{CS} are significant, the PGSE attenuation is no longer dominated by the spins in pores C and pores S only. Instead, the effect of spin diffusion from pores C(S) into pores S(C) is considered (see Eq. 9). In those cases, the $\exp(\lambda_1\Delta)$ versus qb plot is presented in Fig. 2 A, and the $\exp(\lambda_2\Delta)$ versus qb plot is presented in Fig. 2 B. We can clearly see that $\exp(\lambda_1\Delta)$ oscillates with the same periods as $\exp(\lambda_2\Delta)$ does. The position of the first peak of $\exp(\lambda_1\Delta)$ and $\exp(\lambda_2\Delta)$ is situated at qb = 0.72, which is close to $qb = 0.57$ ($qd = q \cdot \sqrt{3}\, b \approx 1$). As compared with the PGSE results for the diffusion among pores of the same size, the position is characterized by the length between two pores S, or two pores C.

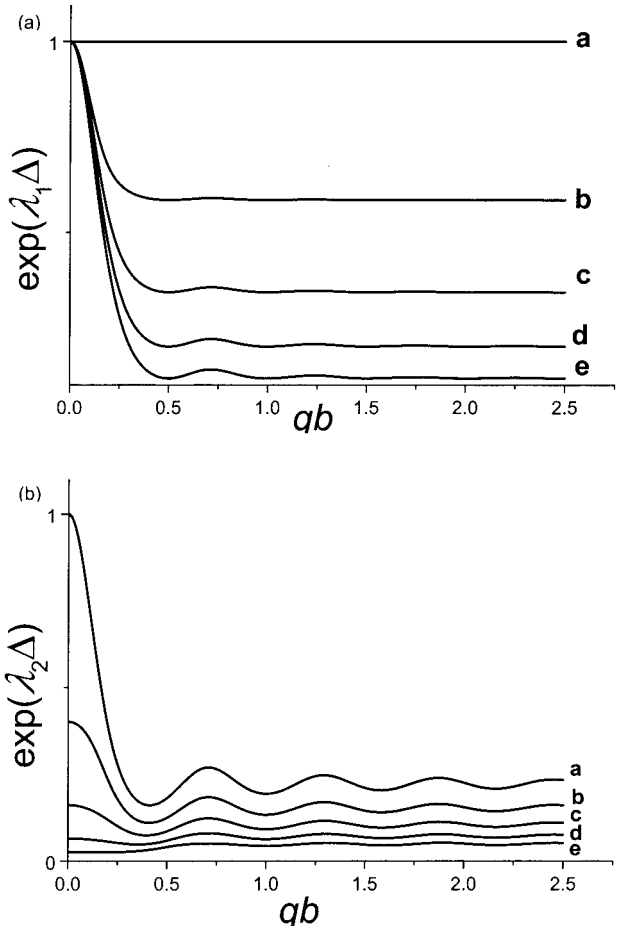

FIGURE 2 The two exponential terms as expressed in Eq. 9 versus qb plots. (A) $\exp(\lambda_1\Delta)$ versus qb plot; (B) $\exp(\lambda_2\Delta)$ versus qb plot. The solid curves a, b, c, d, and e correspond to NW_{SC}/MW_{SS} = 0, 0.25, 0.50, 0.75, and 1.00, respectively.

The increasing oscillation magnitude of the $\exp(\lambda_1\Delta)$ term with increasing W_{SC} and W_{CS} shows the effect of the pore arrangement with the exchange process.

The $E(q, \Delta)$ versus qb curves with different NW_{CS} values are plotted in Fig. 3. The individual contribution to the magnetization, e.g., $M_{C\to C}$, $M_{C\to S}$, $M_{S\to C}$, and $M_{S\to S}$ for three cases, NW_{SC}/MW_{SS} = 0, 0.5, and 1.0, are shown in Fig. 4 for comparison. Apparently, in Fig. 3, there are characteristic peaks at qR_C or $qR_S \approx q \cdot (b/2) \approx 1$ for all of the five curves with various magnitudes of NW_{SC}. The intensity of the characteristic peak decreases as the permeability increases. As shown in Fig. 4, the PGSE attenuation may be analyzed in detail as follows. The characteristic peaks result mainly from $M_{C\to C}$, but not from $M_{S\to S}$, because the high molecular mobility of the spins in pores S causes more attenuation of $M_{S\to S}$ in **q** space. Analogously, the intensity of the characteristic peak in $M_{C\to C}$ decreases with increasing W_{SC} (W_{CS}), which reduces the intensity of the characteristic peak in $E(q, \Delta)$. The increasing decay rate of $E(q, \Delta)$ at small q

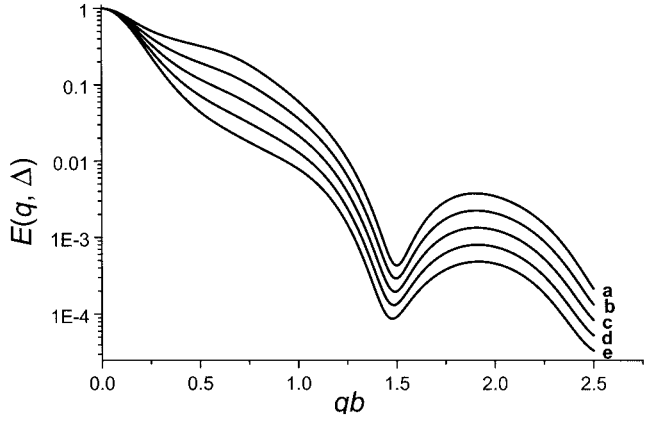

FIGURE 3 The PGSE attenuation E(q, Δ) versus qb plot. The solid curves a, b, c, d, and e correspond to NW_{SC}/MW_{SS} = 0, 0.25, 0.50, 0.75, and 1.00, respectively.

with increasing W_{SC} (W_{CS}) comes mainly from the change of the relative proportion of each component. As shown in Fig. 4 A, $M_{C\to C}$ decreases with increasing W_{SC} (W_{CS}), whereas the fast decaying $M_{C\to S}$, $M_{S\to C}$, and $M_{C\to C}$ dominate the shape of the curve at small q. In addition, when W_{SC} (W_{CS}) is about the same magnitude of W_{SS}, i.e., NW_{SC}/MW_{SS} = 1.0, represented by the dotted line in Fig. 4 A, there is also a fast decay in $M_{C\to C}$ at small qb. When $NW_{SC}/MW_{SS} < 0.5$, because $M_{C\to C}$ is large, the first diffraction-like pattern of $M_{S\to S}$, reflecting the distance between two pores S, is under the shadow of $M_{C\to C}$, and therefore it is invisible on the E(q, Δ)–qb plot.

Orientation effect

For a nonspherical cell suspension system, the orientations of the cells may affect the PGSE attenuation. As shown in Fig. 5, we may consider the disk-shape cells (pores C) suspension system with disk thickness t_1, radius R_1 and the spacing between the cells x. The cells are randomly packed. We may then simply take the averaged shape of the medium (pores S) separating the cells as a disk with radius R_S and thickness t_S estimated from the lattice model shown in Fig. 5 B. The PGSE attenuation for a specific cell orientation θ (see Fig. 5 A) may be derived as

$$E(q, \Delta, \theta) = \frac{1}{V_C + V_S} \times \left\{ \left[\frac{x_{CC}}{V_C} F_C^2(\theta) + \left(\frac{x_{SC}}{V_S} + \frac{x_{CS}}{V_C} \right) F_C(\theta) F_S(\theta) + \frac{x_{SS}}{V_S} F_S^2(\theta) \right] \exp(\lambda_1 \Delta) + \left[\frac{y_{CC}}{V_C} F_C^2(\theta) + \left(\frac{y_{SC}}{V_S} + \frac{y_{CS}}{V_C} \right) F_C(\theta) F_S(\theta) + \frac{y_{SS}}{V_S} F_S^2(\theta) \right] \exp(\lambda_2 \Delta) \right\}, \quad (14)$$

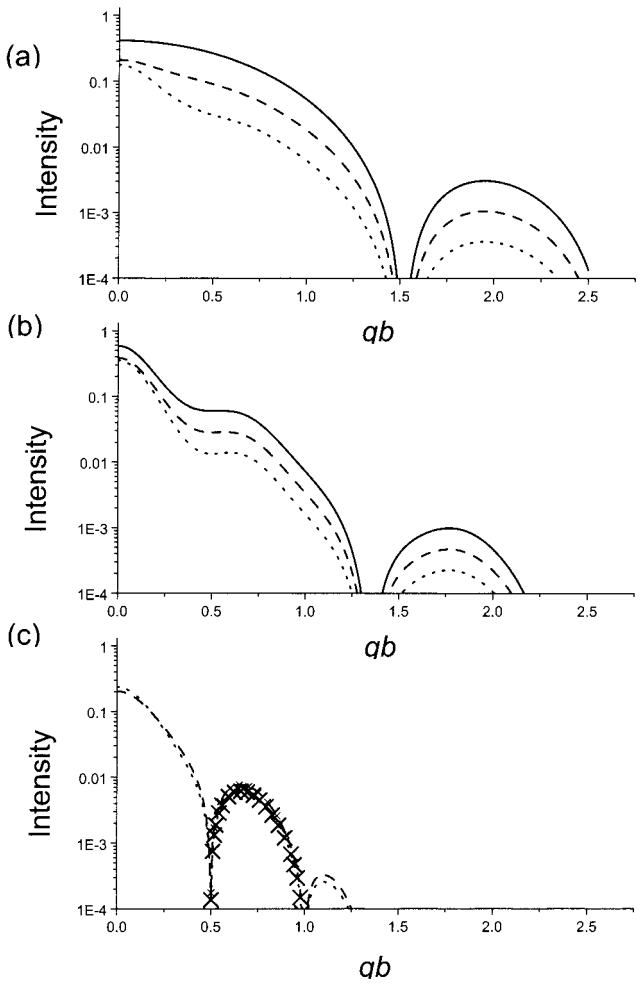

FIGURE 4 The magnetization contributed from each part of the spins with varying NW_{SC}. (A) $M_{C\to C}$, (B) $M_{S\to S}$, (C) $M_{C\to S}$ and $M_{S\to C}$. *Solid lines*, NW_{SC} = 0; *dashed lines*, NW_{SC}/MW_{SS} = 0.5; *dotted lines*, NW_{SC}/MW_{SS} = 1.0. There are two features in (C): 1) there is no contribution of $M_{C\to S}$ and $M_{S\to C}$ for the case of NW_{SC} = 0; and 2) the values in the arch with x on it are the absolute values of the negative calculated results.

where the cell orientation θ is defined as the angle between the magnetic field and the central axis of the pore C. Other parameters have been defined previously for Eq. 9. The structure integral, $F_C(\theta)$, for a pore C with the cell orientation θ is expressed by

$$F_C(\theta) = \int_{v_1} \exp(i 2\pi \mathbf{q} \cdot \mathbf{r}_1) d\mathbf{r}_1 = \frac{t_1 \cdot \mathrm{sinc}[(\pi q t_1 \cos\theta)] \cdot 2\pi R_1 J_1(2\pi q \sin\theta \cdot R_1)}{2\pi q \sin\theta}, \quad (15)$$

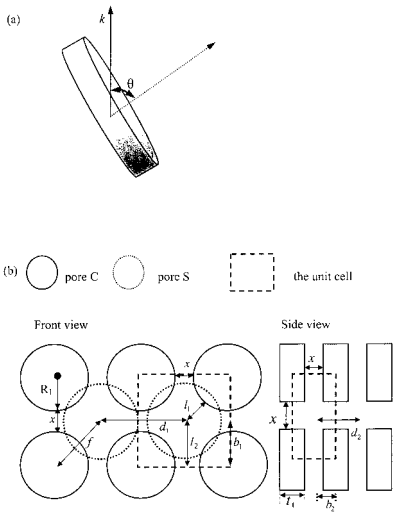

FIGURE 5 (a) The cell orientation θ is defined as the angle between the magnetic field direction (**q** direction) and the central axis of the cell. (b) The lattice model of the equally separated disk-shaped cells with disk radius R_1 and thickness t_1. The averaged shape of the medium (pores S) can be approximated as a disk with radius R_S and thickness t_S. There is one pair of pore C and pore S in a unit cell. The distance between a pore C and a pore S is denoted by b. The distance between two pores S is denoted by d. The distance between cells is denoted by x. R_S is the radius of a pore S. $b = \sqrt{(b_1\cos\theta)^2 + (b_2\sin\theta)^2}$, $d = \sqrt{(d_1\cos\theta)^2 + (d_2\sin\theta)^2}$, $R_S = (l_1 + l_2)/2$, $l_1 = \sqrt{2}\, b_1 - R_1$, $l_2 = b_1$.

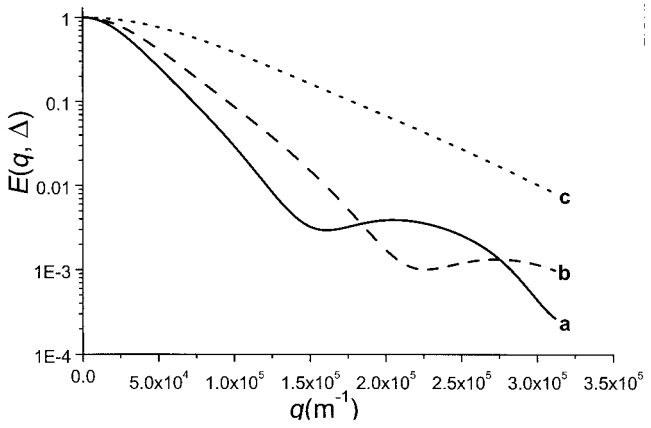

FIGURE 6 The PGSE attenuation E(q, Δ) versus q plot. The curves a, b, c represent the simulation data of a 51% hematocrit erythrocyte suspension at $\theta = 90°$, $\theta = 45°$ and $\theta = 0°$, respectively. The simulation parameters for *curve a*, $a = 3.06\ \mu$m, $b = 4.12\ \mu$m, and $d = 8.24\ \mu$m; *curve b*, $a = 3.06\ \mu$m, $b = 3.1\ \mu$m, and $d = 6.2\ \mu$m; and *curve c*, $a = 3.06\ \mu$m, $b = 1.51\ \mu$m, and $d = 3.01\ \mu$m. The parameters $NW_{CS} = 100\ s^{-1}$ and $MW_{SS} = 120\ s^{-1}$ are for all three curves.

where $J_1(2\pi q \sin\theta \cdot R_1)$ is the first-order Bessel function of the first kind. Similarly, the structure integral, $F_S(\theta)$, for a pore S with the specific cell orientation θ may be expressed as

$$F_S(\theta) = \frac{t_S \cdot \mathrm{sinc}(\pi q t_s \cos\theta) \cdot t_s]2\pi R_S J_1(2\pi q \sin\theta \cdot R_S)}{2\pi q \sin\theta}. \quad (16)$$

To demonstrate the effect of the cells orientation, we may consider the case of $R_1 = 1.5l$, $t_1 = l$ and $x = l/4$ where the length, l, is arbitrary. We then set $\Delta = 1.5/MW_{SS}$ and $NW_{SC} = MW_{SS}$. The PGSE attenuation of different cell orientations versus ql plot is presented in Fig. 6. We can find that the characteristic peak shifts from $ql = 0.56$ to a higher ql value while the cell orientation changes from 90° to 45°. The characteristic peak shifts to an even higher ql value while $\theta = 0°$ and cannot be seen in the low ql region. Moreover, the PGSE signal attenuates slower in the low ql region while $\theta = 0°$ as compared to the cases of $\theta = 90°$ and $\theta = 45°$. The effects of cell orientation merit attention.

Observation of erythrocyte orientation

As shown in Fig. 7 A, pure erythrocytes are oriented with their disk plane parallel to the magnetic field direction. For the controlled experiments in the absence of magnetic field, the erythrocyte orientations were random. These results were the same as those obtained by Higashi et al. (1993). Besides, Kuchel et al. (2000) used the diffusion tensor method to analyze the PGSE attenuation of the erythrocyte suspension system, and they found that the diffusion tensor component at z-direction (the direction parallel to the magnetic field of the NMR spectrometer) is larger, which also verifies the anisotropic orientations of the erythrocytes. The erythrocytes with p-CMBS added, as shown in Fig. 7 B, are oriented with their disk plane perpendicular to the magnetic field direction.

Applications to the erythrocyte suspension system

Experimental PGSE results

Erythrocyte suspension systems prepared as described in Materials and Methods were considered as model cell suspension systems. Here, we have repeated the PGSE experiments of the erythrocyte suspension system studied by Kuchel et al. (1997) but with enhancement of the magnetic field gradient. The PGSE attenuation curve in the **q** space plot is shown in Fig. 8. For the pure erythrocyte suspension system, we performed PGSE experiments with $\delta = 1.2$ ms and $\delta = 2$ ms. These two experiments showed the same results in PGSE experiments; short gradient pulse approximation may be applied accordingly. For the system of erythrocyte suspension with p-CMBS added, the PGSE signal attenuates more slowly than that of a pure erythrocyte suspension system. Moreover, there was no characteristic peak found (see Fig. 8). These two features may account for the change of erythrocyte orientation as compared to those of the orientation effects. The results of the erythrocyte

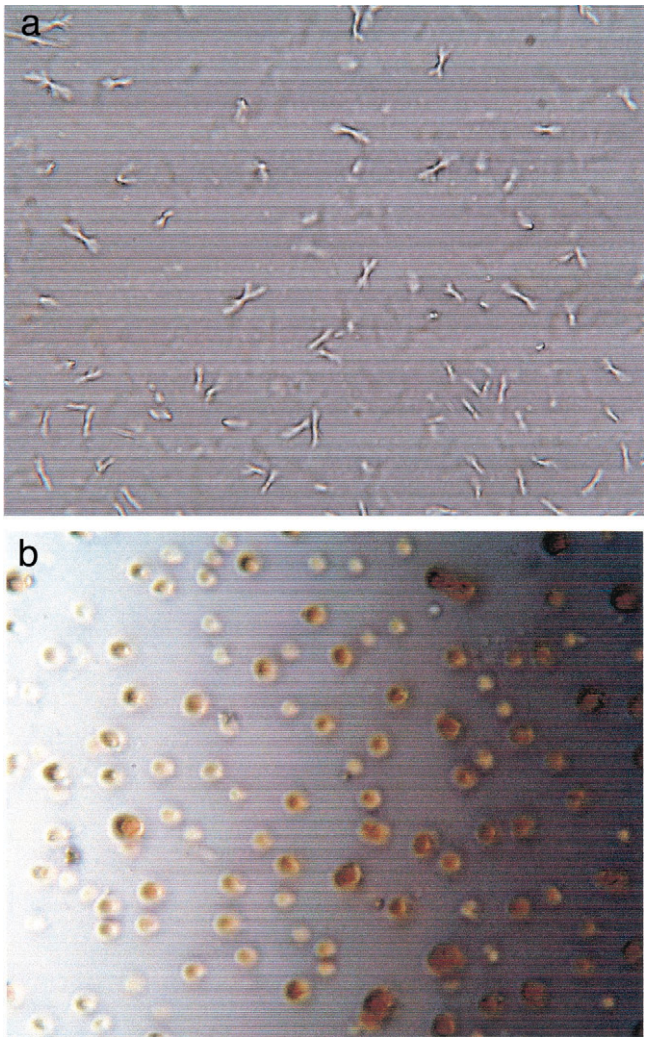

FIGURE 7 (a) Pure erythrocytes and (b) erythrocytes with p-CMBS added inside a 11.4-T magnetic field. The magnetic field direction is normal to the test plane. Pure erythrocytes were photographed on their edge so that they were orientated with their disk plane parallel to the magnetic field direction. Erythrocytes with p-CMBS added were photographed on their edge so that they were orientated with their disk plane normal to the magnetic field direction. For the controlled experiments in the absence of magnetic field, the erythrocyte orientations were random. The controlled results were the same as those obtained by Higashi et al. (1993).

orientation were observed by light microscope, confirming this prediction.

Analysis of the experimental results

The disk-shaped cell suspension model can be used to analyze the PGSE experimental results. The erythrocytes can be approximated as a biconcave disk (Beck, 1978; Higashi et al. 1993; Kuchel et al., 1997) with diameters ranging from 6.7 to 8.7 μm. To take into account the differences in the erythrocytes radii, we then

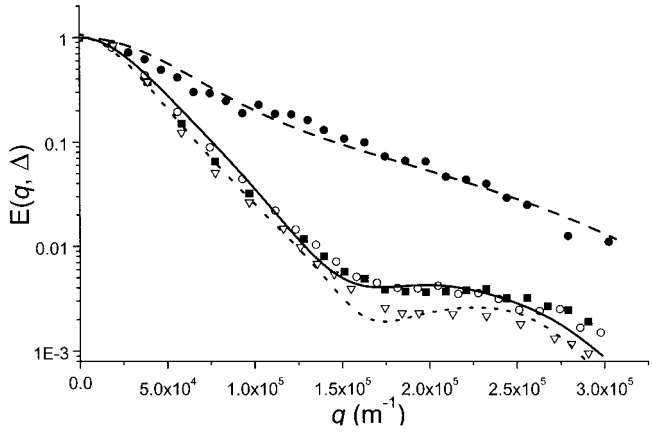

FIGURE 8 The experimental PGSE attenuation $E(q, \Delta)$ versus q plot and the simulated results. *Solid circles* and *dashed line* stand for the experimental and fitted results, respectively, for the 48% hematocrit erythrocyte suspension with p-CMBS added (NMR parameters: $\delta = 1.2$ ms and $\Delta = 40$ ms). *Open circles* and *solid squares* stand for the experimental result of $\delta = 2$ ms and $\delta = 1.2$ ms, respectively, for the 51% hematocrit pure erythrocyte suspension. *Solid line* is the fitted result for 51% hematocrit pure erythrocyte suspension. The time interval of the two gradient pulses was set to 15 ms. *Open inverted triangles* and *dotted line* stand for the experimental and fitted results, respectively, for the 40% hematocrit pure erythrocyte suspension (NMR parameters: $\delta = 2$ ms and $\Delta = 40$ ms).

consider that the radii of erythrocytes follow the distribution

$$P(R_1) = N_C \exp[-(R_1 - R_m)^2/2\sigma^2], \tag{17}$$

where $R_m = 3.85$ μm is the mean radius and $\sigma = 0.5$ μm is the standard deviation of radius distribution. Thus, by considering the radius distribution of erythrocytes, the PGSE attenuation can be modified from Eq. 14 as

$$\tilde{E}(q, \Delta, \theta) = \sum_{R_1} P(R_1) E(q, \Delta, \theta, R_1), \tag{18}$$

where

$$E(q, \Delta, \theta, R_1) = \frac{1}{\rho_W V_C + V_S} \times \left\{ \left[\rho_W \frac{x_{CC}}{V_C} F_C^2(R_1, \theta) + \left(\rho_W \frac{x_{SC}}{V_S} + \frac{x_{CS}}{V_C} \right) F_C(R_1, \theta) F_S(R_1, \theta) + \frac{x_{SS}}{V_S} F_S^2(R_1, \theta) \right] \exp(\lambda_1 \Delta) + \left[\rho_W \frac{y_{CC}}{V_C} F_C^2(R_1, \theta) + \left(\rho_W \frac{y_{SC}}{V_S} + \frac{y_{CS}}{V_C} \right) F_C(R_1, \theta) F_S(R_1, \theta) + \frac{y_{SS}}{V_S} F_S^2(R_1, \theta) \right] \exp(\lambda_2 \Delta) \right\} \tag{19}$$

Here $F_S(R_1, \theta)$ means that the size and the structural integral of an external pore depends on the radius of the erythrocyte in each subsystem, because the hematocrit value is set to be constant in all of the subsystems. It is known that the density

of the erythrocyte is almost the same as that of the outer medium, and the weight percentage of water ρ_W in the erythrocyte is about 70% (Grimes, 1980). In addition, for a constant hematocrit value, as R_1 varies according to the Gaussian distribution, Eq. 17, it is noted that the radius a of the external pore follows linearly with the relation, $(a - a_m)/a_m = (R_1 - R_m)/R_m$, where a_m is the mean value of a. All other parameters in Eq. 19 have been defined already in the previous sections.

As shown in Fig. 9, considering the shape of erythrocyte, according to the definition of the structure integral for a pore C, it can be calculated as

$$\begin{aligned} F_C(R_1, \theta) &\equiv \int_{V_C} \exp(i2\pi q \cdot r_C)\mathrm{d}r_C \\ &= \int_{\nu_1} \exp(i2\pi q \cdot r_1)\mathrm{d}r_1 - \int_{\nu_2} \exp(i2\pi q \cdot r_2)\mathrm{d}r_2 \\ &\quad + \int_{\nu_3} \exp(i2\pi q \cdot r_3)\mathrm{d}r_3 \\ &= \frac{t_1 \cdot \sin c[(2\pi q \cos\theta/2) \cdot t_1] \cdot 2\pi R_1 J_1(2\pi q \sin\theta R_1)}{2\pi q \sin\theta} \\ &\quad - \frac{t_1 \cdot \sin c[(2\pi q \cos\theta/2) \cdot t_1] \cdot 2\pi R_2 J_1(2\pi q \sin\theta R_2)}{2\pi q \sin\theta} \\ &\quad + \frac{t_2 \cdot \sin c[(2\pi q \cos\theta/2) \cdot t_2] \cdot 2\pi R_2 J_1(2\pi q \sin\theta R_2)}{2\pi q \sin\theta}. \end{aligned} \tag{20}$$

The fitting parameters are described as follows. The ratio of W_{CS} to W_{SC} is obtained by the principle of detailed balance $P_C W_{CS} = P_S W_{SC}$, where P_C and P_S are the populations of the water inside and outside the erythrocytes, respectively. The ratio is given by $P_C{:}P_S = \rho_W h{:}(1 - h)$ because the hematocrit value h is defined as the ratio of the volume of a disk and the volume of the total suspension.

Because the shape of the erythrocyte resembles a disk, the mean distance between pore C and pore S and that between two pore S are not as easily described as in the case of the spherical-cell suspension. Therefore, we constructed a periodically stacked structure for pore C and pore S, as shown in Fig. 5 B, where the distances between all pairs of pores C are the same. By the definition of the hematocrit content, $h = V_C/V_{u.c.}$, the spacing x between the erythrocytes may be evaluated. For 40% (or 51%) hematocrit, it yields $x = 0.98$ μm (or 0.54 μm). This is about the size of the channel between pores, which is small compared to the diameter of erythrocyte, $R_1 = 7.7$ μm and to that of pore S, $a = 6.6$ μm (or 6.1 μm). The differences between the sizes of channel and the pore confirm the validity of pore equilibrium conditions. Moreover, the estimations of the averaged values of distance parameters b (the distance between the adjacent pore C and pore S), d (the distance between two adjacent pores S), and the mean size a_m of a pore S can also be made from this model. The results for different erythrocyte solutions are listed in Table 1.

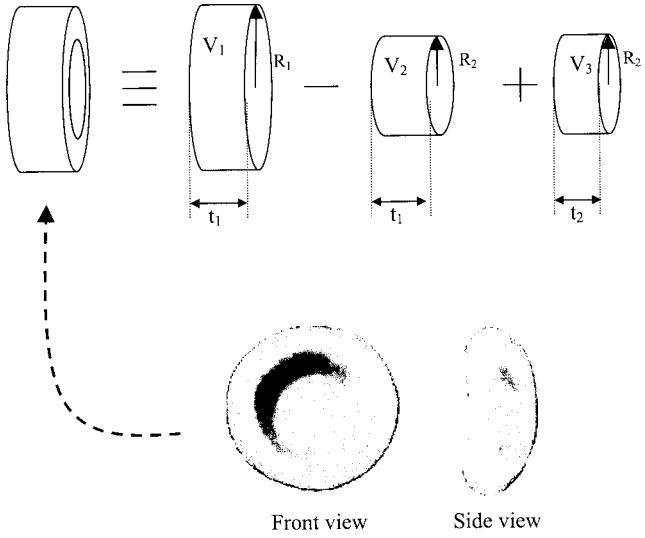

FIGURE 9 The side view and the front view of the erythrocyte and the approximated shape of the erythrocyte.

For the pure erythrocyte suspension system, the erythrocytes preferably align with a magnetic field of 11.4 T (Higashi et al. 1993). Then the orientation was determined as $\theta = 90°$. Finally, only the hopping rates, MW_{SS}, NW_{CS}, and NW_{SC}, remain to be determined, and only either NW_{CS} or NW_{SC} needs to be solved, according to the detailed balance principle.

Based on the theoretical analysis, the hopping rate NW_{SS} between pores S, which represents the diffusivity of water outside the erythrocytes, can be determined from the slope of the early part, i.e., the fast-decaying part of the curve. The hopping rates NW_{SC} and NW_{CS} between the two phases may be calculated from the intensities of the slow-decaying part of the curve and the characteristic peak. For the erythrocyte suspension with p-CMBS added, as mentioned previously, the erythrocyte orientation becomes normal to the magnetic field direction, so we can set $\theta = 0°$. In the two cases ($\theta = 0°$ and 90°), the hopping rate NW_{SS} was kept unchanged, and the hopping rate NW_{SC} varies to fit the result, whereas the water residence times τ_C inside an erythrocyte correspond to the inverse of the fitting parameter NW_{CS}.

The fitting results are shown in Fig. 8, and all the fitting parameters are listed in Table 1. In addition, the magnetization contributed from each part of the spins in the 51% and 40% hematocrit erythrocyte suspensions are shown in Figs. 10 and 11, respectively. From Figs. 10 and 11, it is obvious that the slow decaying is attributed to both $M_{C\to C}$

TABLE 1 Results of fitting the experimental PGSE attenuation curves of pure erythrocyte suspensions and the erythrocyte suspension with p-CMBS added

	Predefined Parameters				Fitted Parameters	
Sample	θ	a_m* (μm)	b (μm)	d (μm)	MW_{SS} (s^{-1})	NW_{CS} (s^{-1})
Pure erythrocyte suspension (Ht = 51%)	90°	3.05	4.12	8.24	110	90
Pure erythrocyte suspension (Ht = 40%)	90°	3.31	4.34	8.68	110	110
Erythrocyte suspension with p-CMBS (Ht = 48%)	0°	3.09	1.54	3.05	140	35

*a_m is the mean radius of an external pore, and the radius of an external pore is proportional to the radius of an erythrocyte in the simulation program.

and $M_{S\to S}$, i.e., the signal intensity from the water inside the erythrocytes and the external pores. That is, the diffraction-like pattern at low q ($\approx 10^5\ m^{-1}$), which is indicative of the mean distance between two pores S as proposed by Kuchel et al. (1997), is actually caused by the combination of the restricted diffusion between multi-external pores and the restricted diffusion within the erythrocytes. In addition, the lifetime of the water in the erythrocyte τ_C is equal to $1/NW_{CS}$ according to the definition in Eq. 8a (or 8b), thus τ_C ranges from 9 to 11 ms, which is close to the mean value of 10 ms obtained from the original two-phase exchange model without considering the restriction effect (Andrasko, 1976) and also close to that obtained from the modified two-phase model when including the restricted effect (Stanisz et al., 1998). In other words, the same exchange rate can be obtained by one of the three models, but the diffraction-like peak caused by the restricted diffusion can only be interpreted by the modified two-phase model and ours. However, our model can be used to investigate the restricted diffusion between external pores connecting to each other, which is especially useful when the cells in a cell suspension are concentrated enough to generate the pore-like external space. The sufficient cell concentration for a cell suspension is necessary if one wants to measure the weak diffraction-like peak and obtain directly the size of the cell from the position of the diffraction-like peak.

APPENDIX

One may solve $C(\mathbf{q}, \Delta)$ and $S(\mathbf{q}, \Delta)$ with the help of the Fourier–Laplace transform of Eqs. 8a and 8b. We obtain

$$sC[\mathbf{q}, s] - C(\mathbf{q}, t = 0) = W_{SC}\sum_{i=1}^{N}\exp(i2\pi\mathbf{q}\cdot\mathbf{R}_{SCi})S[\mathbf{q}, s] - NW_{CS}C[\mathbf{q}, s], \tag{A1a}$$

$$sS[\mathbf{q}, s] - S(\mathbf{q}, t = 0) = W_{SS}\sum_{i=1}^{M}\exp(i2\pi\mathbf{q}\cdot\mathbf{R}_{SSi})S[\mathbf{q}, s] + W_{CS}\sum_{i=1}^{N}\exp(i2\pi\mathbf{q}\cdot\mathbf{R}_{CSi})C[\mathbf{q},s] - (NW_{SC} + MW_{SS})S[\mathbf{q}, s], \tag{A1b}$$

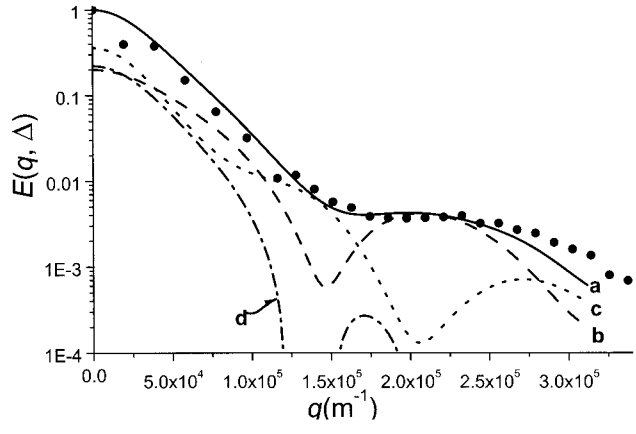

FIGURE 10 The magnetization contributed from each part of the spins in the 51% hematocrit erythrocyte suspension, and the experimental PGSE attenuation $E(q, \Delta)$ versus q plot (*solid circles*) and the simulated results. (*a*) $E(q, \Delta)$, (*b*) $M_{C\to C}$, (*c*) $M_{S\to S}$, (*d*) $M_{C\to S}$ and $M_{S\to C}$.

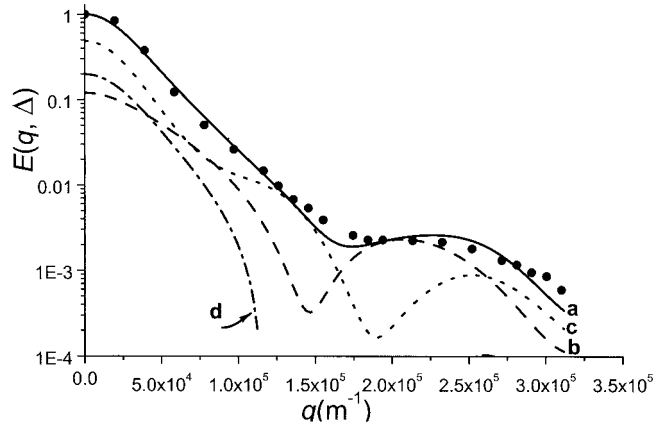

FIGURE 11 The magnetization contributed from each part of the spins in the 40% hematocrit erythrocyte suspension, and the experimental PGSE attenuation $E(q, \Delta)$ versus q plot (*solid circles*) and the simulated results. (*a*) $E(q, \Delta)$, (*b*) $M_{C\to C}$, (*c*) $M_{S\to S}$, (*d*) $M_{C\to S}$ and $M_{S\to C}$.

where $\mathbf{R}_{XYi}(X, Y = S, C)$ is the position vector at the center of the ith neighboring pore X relative to that of the central pore Y. The arrangement of pores C and pores S must be defined for the calculations of the three configuration integrals in Eqs. A1a and A1b. Considering the nature of a cell suspension system, the stacking of pores C and pores S is presumably random. If the distance between a pair of neighboring pore C and S is b, and that between two neighboring pores S is d (see Fig. 1), the mean configuration integrals in Eqs. A1a and A1b for the randomly packed pores are

$$\left\langle \sum_{i=1}^{N} \exp(i2\pi\mathbf{q}\cdot\mathbf{R}_{CSi}) \right\rangle = N\cdot \mathrm{sinc}(2\pi qb)$$

and

$$\left\langle \sum_{i=1}^{M} \exp(i2\pi\mathbf{q}\cdot\mathbf{R}_{SSi}) \right\rangle = M\cdot \mathrm{sinc}(2\pi qd)$$

(Callaghan et al., 1991). If the spin initially exists in a given pore A with its center at origin (case A), the initial condition is

$$C(\mathbf{q}, t=0) = 1\cdot\exp(i2\pi\mathbf{q}\cdot 0) = 1,$$
$$S(\mathbf{q}, t=0) = \sum_{n} 0\cdot\exp(i2\pi\mathbf{q}\cdot\mathbf{R}_{Sn}) = 0$$

according to Eq. 4, where $\mathbf{R}_{Sn}$ is the center of the nth pore S. Similarly, if a spin exists at a pore S at the initial time $t = 0$ (case B), the initial condition yields $C(\mathbf{q}, t = 0) = 0$ and $S(\mathbf{q}, t = 0) = 1$. Because the present system is isotropic, $C(\mathbf{q}, t)$ and $S(\mathbf{q}, t)$ can be replaced by $C(q, t)$ and $S(q, t)$. Eqs. A1a and A1b then reduce to

$$(s + NW_{CS})C[q, s] - N\,\mathrm{sinc}(2\pi qb)W_{SC}S[q, s] = C(q, t=0) = \begin{cases} 1 & \text{for case A} \\ 0 & \text{for case B} \end{cases} \quad \text{(A2a)}$$

$$-N\,\mathrm{sinc}(2\pi qb)W_{CS}C[q, s] + (s + \alpha)S[q, s] = S(q, t=0) = \begin{cases} 0 & \text{for case A} \\ 1 & \text{for case B} \end{cases} \quad \text{(A2b)}$$

where

$$\alpha = NW_{SC} + MW_{SS}[1 - \mathrm{sinc}(2\pi qd)]. \quad \text{(A3)}$$

The solutions of the coupled Eqs. A2a and A2b are given by

$$C_C[q, s] = \frac{x_{CC}}{(s-\lambda_1)} + \frac{y_{CC}}{(s-\lambda_2)},$$
$$x_{CC} \equiv \frac{\lambda_1 + \alpha}{\lambda_1 - \lambda_2}, \quad y_{CC} \equiv \frac{\lambda_2 + \alpha}{\lambda_2 - \lambda_1}, \quad \text{(A4a)}$$

$$S_C[q, s] = \frac{x_{SC}}{(s-\lambda_1)} + \frac{y_{SC}}{(s-\lambda_2)},$$
$$x_{SC} \equiv \frac{NW_{CS}\cdot\mathrm{sinc}(2\pi qb)}{\lambda_1 - \lambda_2}, \quad \text{(A4b)}$$
$$y_{SC} \equiv \frac{NW_{CS}\cdot\mathrm{sinc}(2\pi qb)}{\lambda_2 - \lambda_1},$$

$$C_S[q, s] = \frac{x_{CS}}{(s-\lambda_1)} + \frac{y_{CS}}{(s-\lambda_2)},$$
$$x_{CS} \equiv \frac{NW_{SC}\cdot\mathrm{sinc}(2\pi qb)}{\lambda_1 - \lambda_2}, \quad \text{(A4c)}$$
$$y_{CS} \equiv \frac{NW_{SC}\cdot\mathrm{sinc}(2\pi qb)}{\lambda_2 - \lambda_1},$$

$$S_S[q, s] = \frac{x_{SS}}{(s-\lambda_1)} + \frac{y_{SS}}{(s-\lambda_2)},$$
$$x_{SS} \equiv \frac{\lambda_1 + NW_{CS}}{\lambda_1 - \lambda_2}, \quad y_{SS} \equiv \frac{\lambda_2 + NW_{CS}}{\lambda_2 - \lambda_1}, \quad \text{(A4d)}$$

where

$$\lambda_{1,2} \equiv \frac{-(NW_{CS} + \alpha) \pm \sqrt{(NW_{CS} - \alpha)^2 + 4N^2W_{CS}W_{SC}\mathrm{sinc}^2(2\pi qb)}}{2}. \quad \text{(A5)}$$

$C_C(q, \Delta)$, $S_C(q, \Delta)$, $C_S(q, \Delta)$, and $S_S(q, \Delta)$ can be obtained by the inverse Laplace transform of $C_C[q, s]$, $S_C[q, s]$, $C_S[q, s]$, and $S_S[q, s]$; then the four parts of the magnetizations, $M_{C\to C}$, $M_{C\to S}$, $M_{S\to C}$, and $M_{S\to S}$, may be calculated in accordance with Eq. 6. By summing the four parts, we obtain the PGSE attenuation $E(q, \Delta)$ as given in Eq. 12.

REFERENCES

Andrasko, J. 1976. Water diffusion permeability of human erythrocytes studied by a pulsed gradient NMR technique. *Biochim. Biophys. Acta.* 428:304–311.

Balinov, B., O. Söderman, and J. C. Ravey. 1994. Diffraction-like effects observed in the PGSE experiment when applied to a highly concentrated water/oil emulsion. *J. Phys. Chem.* 98:393–395.

Barzykin, A. V., K. Hayamizu, W. S. Price, and M. Tachiya. 1995. Pulsed-field-gradient NMR of diffusive transport through a spherical interface into an external medium containing a relaxation agent. *J. Magn. Reson. A.* 114:39–46.

Beck, J. S. 1978. Relations between membrane monolayer in some red cell shape transformations. *J. Theor. Biol.* 75:487–501.

Callaghan, P. T. 1991. Principles of Nuclear Magnetic Resonance Microscopy. Chap. 7. Clarendon Press, Oxford.

Callaghan, P. T., A. Coy, D. MacGowan, K. J. Packer, and F. O. Zelaya. 1991. Diffraction-like effects in NMR diffusion studies of fluids in porous solids. *Nature.* 351:467–469.

Callaghan, P. T. 1995. Pulsed-gradient spin-echo NMR for planar, cylindrical, and spherical pores under conditions of wall relaxation. *J. Magn. Reson. A.* 113:53–59.

Codd, S. L., and P. T. Callaghan. 1999. Spin echo analysis of restricted diffusion under generalized gradient waveforms: planar, cylindrical, and spherical pores with wall relaxivity. *J. Magn. Reson.* 137:358–372.

Grimes, A. J. 1980. Human Red Cell Metabolism. Blackwell Scientific Publications, Oxford, London, pp. 179–180.

Haus, J. W., K. W. Kehr. 1987. Diffusion in regular and disordered lattices. *Phys. Rep.* 150:263–406.

Higashi, T., A. Yamagishi, T. Takeuchi, and N. Kawaguchi. 1993. Orientation of erythrocytes in a strong static magnetic field. *Blood.* 82: 1328–1334.

Kärger, J. 1985. NMR self-diffusion studies in heterogeneous systems. *Adv. Colloid Interface Sci.* 23:129–148.

Kuchel, P. W., A. Coy, and P. Stilbs. 1997. NMR "diffusion-diffraction" of water revealing alignment of erythrocytes in a magnetic field and their dimensions and membrane transport characteristics. *Magn. Reson. Med.* 37:637–643.

Kuchel, P. W., C. J. Durrant, B. E. Chapman, P. S. Jarrett, and D. G. Regan. 2000. Evidence of red cell alignment in the magnetic field of an NMR spectrometer based on the diffusion tensor of water. *J. Magn. Reson.* 145:291–301.

Linse, P., and O. Söderman. 1995. The validity of the short-gradient-pulse approximation in NMR studies of restricted diffusion. Simulations of molecules diffusing between planes, in cylinders and spheres. *J. Magn. Reson. A.* 116:77–86.

Peled, S., D. G. Cory, S. A. Raymond, D. A. Kirschner, and F. A. Jolesz. 1999. Water diffusion, T_2, and compartmentation in frog sciatic nerve. *Magn. Reson. Med.* 42:911–918.

Price, W. S., A. V. Barzykin, K. Hayamizu, and M. Tachiya. 1998. A model for diffusive transport through a spherical interface probed by pulsed-field gradient NMR. *Biophys. J.* 74:2259–2271.

Stanisz, G. J., J. G. Li, G. A. Wright, R. M. Henkelman. 1998. Water dynamics in human blood via combined measurements of T_2 relaxation and diffusion in the presence of gadolinium. *Magn. Reson. Med.* 39:223–233.

Tanner, J. E., and E. O. Stejskal. 1968. Restricted self-diffusion of protons in colloidal systems by the pulse-gradient, spin-echo method. *J. Chem. Phys.* 49:1768–1777.